

1
2 **Supplementary Materials for**

3 Ancient chicken remains reveal the origins of virulence in Marek's disease virus

4
5 **Authors:**

6 Steven R Fiddaman^{1†*}, Evangelos A Dimopoulos^{2,3†}, Ophélie Lebrasseur^{4,5}, Louis du Plessis^{6,7}, Bram
7 Vrancken^{8,9}, Sophy Charlton^{2,10}, Ashleigh F Haruda², Kristina Tabbada², Patrik G Flammer¹, Stefan
8 Dascalu¹, Nemanja Marković¹¹, Hannah Li¹², Gabrielle Franklin¹³, Robert Symmons¹⁴, Henriette
9 Baron¹⁵, László Daróczi-Szabó¹⁶, Dilyara N Shaymuratova¹⁷, Igor V Askeyev¹⁷, Olivier Putelat¹⁸,
10 Maria Sana¹⁹, Hossein Davoudi²⁰, Homa Fathi²⁰, Amir Saed Mucheshi²¹, Ali Akbar Vahdati²²,
11 Liangren Zhang²³, Alison Foster²⁴, Naomi Sykes²⁵, Gabrielle Cass Baumberg², Jelena Bulatović²⁶,
12 Arthur O Askeyev¹⁷, Oleg V Askeyev¹⁷, Marjan Mashkour^{20,27}, Oliver G Pybus^{1,28}, Venugopal
13 Nair^{1,29}, Greger Larson^{2‡}, Adrian L Smith^{1*‡}, Laurent AF Frantz^{30,31*‡}

14 **Affiliations:**

15 ¹Department of Biology, University of Oxford, Oxford, UK

16 ²The Palaeogenomics & Bio-Archaeology Research Network, Research Laboratory for Archaeology
17 and History of Art, University of Oxford, Oxford, UK

18 ³Department of Veterinary Medicine, University of Cambridge, Cambridge, UK

19 ⁴Centre d' Anthropobiologie et de Génomique de Toulouse, Toulouse, France

20 ⁵Instituto Nacional de Antropología y Pensamiento Latinoamericano, Ciudad Autónoma de Buenos
21 Aires, Buenos Aires, Argentina

22 ⁶Department of Biosystems Science and Engineering, ETH Zurich, Basel, Switzerland

23 ⁷Swiss Institute of Bioinformatics, Lausanne, Switzerland

24 ⁸Department of Microbiology, Immunology and Transplantation, Rega Institute, KU Leuven, Leuven,
25 Belgium

26 ⁹Spatial Epidemiology Lab (SpELL), Université Libre de Bruxelles, Brussels, Belgium

27 ¹⁰BioArCh, Department of Archaeology, University of York, York, UK

28 ¹¹Institute of Archaeology, Belgrade, Serbia

29 ¹²Institute of Immunity and Transplantation, University College London, London, UK

30 ¹³Silkie Club of Great Britain, Charing, UK

- 31 ¹⁴Fishbourne Roman Palace, Fishbourne, UK
- 32 ¹⁵Leibniz-Zentrum für Archäologie, Mainz, Germany
- 33 ¹⁶Medieval Department, Budapest History Museum, Budapest, Hungary
- 34 ¹⁷Laboratory of Biomonitoring, The Institute of Problems in Ecology and Mineral Wealth, Tatarstan
35 Academy of Sciences, Kazan, Russia
- 36 ¹⁸Archéologie Alsace - PAIR, Bas-Rhin, France
- 37 ¹⁹Departament de Prehistòria, Universitat Autònoma de Barcelona, Barcelona, Spain
- 38 ²⁰Bioarchaeology Laboratory, Central Laboratory, University of Tehran, Tehran, Iran
- 39 ²¹Department of Art and Architecture, Payame Noor University (PNU), Tehran, Iran
- 40 ²²Provincial Office of the Iranian Center for Cultural Heritage, Handicrafts and Tourism Organisation,
41 Bojnord, Iran
- 42 ²³Department of Archaeology, School of History, Nanjing University, China
- 43 ²⁴Headland Archaeology, Edinburgh, UK
- 44 ²⁵Department of Archaeology, University of Exeter, Exeter, UK
- 45 ²⁶Department of Historical Studies, University of Gothenburg, Gothenburg, Sweden
- 46 ²⁷CNRS, National Museum Natural History Paris, Paris, France
- 47 ²⁸Department of Pathobiology and Population Sciences, Royal Veterinary College, London, UK
- 48 ²⁹Viral Oncogenesis Group, Pirbright Institute, Woking, UK
- 49 ³⁰Department of Veterinary Sciences, Ludwig Maximilian University of Munich, Munich, Germany
- 50 ³¹School of Biological and Chemical Sciences, Queen Mary University of London, London, UK
- 51 †joint-first author
- 52 ‡ co-senior authors
- 53 * corresponding authors. Emails: steven.fiddaman@biology.ox.ac.uk; adrian.smith@biology.ox.ac.uk;
54 laurent.frantz@lmu.de

55 **This PDF file includes:**

- 56 Materials and Methods
- 57 Supplementary Text
- 58 Figs. S1 to S11

59 Tables S4, S9 and S10

60 Captions for Data S1

61 References (26-74)

62

63 **Other Supplementary Materials for this manuscript include the following:**

64

65 Data S1, which comprises:

- 66 ● Table S1: Sample metadata
- 67 ● Table S2: Screening and capture sequencing results
- 68 ● Table S3: Modern genome metadata
- 69 ● Table S5: Integrity of miRNA sequences in ancient MDV
- 70 ● Table S6: Fixed differences between ancient and modern MDV strains
- 71 ● Table S7: PAML results
- 72 ● Table S8: Meq sequence metadata
- 73 ● Table S11: Metagenomic screening summary data
- 74 ● Table S12: SNP summary table
- 75 ● Table S13: Tip dates for BEAST analysis

76 **Materials and Methods:**

77 Archeological site descriptions

78 1. **Buda Castle**, Teleki Palace, Budapest, Hungary (13th-18th century; OL1385, OL1389;
79 contact: László Daróczy-Szabó).

80 The former Teleki Palace is located in Buda Castle (Castle Hill, Budapest, Hungary), the medieval
81 royal capital of Hungary, in close vicinity of the Royal Palace, in a general height of 158 meters
82 above Baltic Sea level. Excavations of the remains of the palace were directed in 1999-2000 by
83 Dorottya B. Nyékhelyi. Despite the relatively small area, a large number of archeological finds came
84 to the surface, with a large majority dating between the 13th and 18th Century. Among other types of
85 finds at least 100,000 animal remains were excavated (the analysis of the assemblage is ongoing). In
86 general the assemblage shows a typical picture of animal use of the area: cattle dominating with
87 around 45% of the finds, followed by sheep and/or goat and pig (20%), and others. The domination of
88 domestic animals is almost total, although written sources prove that game was an important part of
89 everyday diet: the most likely explanation is that large wild animals were deboned at the hunting site,
90 and only the meat got to the markets. The relatively small number of bird and fish remains is because
91 of the excavation methods: most of the finds were hand collected, and only a small part went through
92 water sieving – here the number of these small finds drastically increased. Discrepancy from this
93 generalities could be observed when finds connected to non-christian population were examined: pig
94 is almost totally non-existent in layers supposedly connected to the local, 14th Century Jewish
95 population of “Well 8”, and objects from the Ottoman Period (mid 16th-late 17th Century) (e.g. “Well
96 7”). In the latter next to the lack of pig remains a drastic increase of domestic small ruminants was
97 noticed, as well as a decrease in cattle remains, the former becoming dominant.

98
99 2. **Castillo de Montsoriu**, Spain (16th century; OL1984, OL1986, OL1999; contact: Maria
100 Sana).

101
102 Montsoriu Castle is located in the north-east of the Iberian Peninsula, on a hilltop at 650 m.a.s.l.
103 (4114605800N, 213203000E). Archaeological excavations on-going since 1993 have been able to
104 document the successive changes and re-structuring it underwent from the tenth century onwards, in
105 consonance with the social and political changes in that long span of time. During the 2007 season, an
106 abandoned cistern was excavated. This corresponds to the last stable occupation phase at the castle. It
107 yielded an extremely well-preserved assemblage (UE 10955) consisting of different categories of organic
108 and inorganic remains from the castle's larder. This sample results from a specific action carried out in a
109 very short time. The bone sample recovered from the castle's cistern totals 10,922 remains, being
110 representative of the food stored in the castle's larder. The deposition of this assemblage in the cistern
111 would have been linked with the final abandonment of the castle in the last third of the sixteenth century.
112 The inhabitants of the castle based animal resources exploitation strategies on domestic species (97% of
113 NISP), including sheep and goats (29%), pigs (39%), cattle (32%) and poultry. Hunting was of lesser
114 economic importance, and mainly involved wild rabbits, hares, red deer, boar, roe deer and fox. A large
115 number of birds and fish are also consumed. A total of 863 chicken bones were retrieved from UE10955,

116 representing a total of 74 specimens. Most of the chicken remains correspond to females (61%). A total
117 of 65 chicken remains show cut marks resulting from food processing and cooking for consumption.

118
119 3. **Strasbourg Rue de Lucerne** - Rue du Jeu de Paume, France (16th- early 17th century;
120 OL1936; contact: Olivier Putelat).

121 An archeological excavation was carried out « Rue de Lucerne – Rue du Jeu de Paume », in 2012-
122 2013, in a suburb of the city of Strasbourg (France, Bas-Rhin). This excavation was carried out by the
123 PAIR/Archéologie Alsace, on an area of 1119m², under the direction of M. Werlé. An agro-pastoral
124 building was uncovered, as well as latrines. The site yielded 3,124 terrestrial animal bones, and about
125 1,300 fish remains. The filling of latrines 1067 (US 1059), from which the OL1936 sample originated,
126 is dated to the end of the 16th Century. US 1059 yielded 499 remains of terrestrial animals (NISP:
127 397), including 45 chicken bones (11% of the NISP) and 32 remains of other birds, ducks and geese
128 mainly(26).

129
130 4. **Rudnik**, Serbia (14th-15th century; OL1008; contacts: Nemanja Marković and Jelena
131 Bulatović).

132 The medieval settlement of Rudnik comprises four archaeological sites: Stacionar, Imanje Nikić,
133 Imanje Marković, and Kojovača. The settlement is situated on the Rudnik Mountain, near the present-
134 day town of Rudnik in central Serbia (approx. 95 km south of Belgrade (44°08'06.0"N
135 20°29'42.0"E)). Based on the current archaeological and written records, this area became particularly
136 important in the second half of the 13th century, when German Saxon miners inhabited the country on
137 the invitation of the Serbian king Stefan Uroš I Nemanjić (1241/1242–1276). New technologies in the
138 exploitation and processing of ores provided a significant increase in the economy of medieval Serbia.
139 The established square with an urban settlement developed later into an important mining and trade
140 center, reaching its peak during the 14th and the first part of the 15th century. The main mining activity
141 was the silver extraction, while large amounts of lead and copper were also exploited. Most likely
142 from the very beginning of the mining activities, the mint under the direct management of the Serbian
143 ruler started working at medieval Rudnik. Historical records indicate that a colony of Dubrovnik
144 traders was also established here. So far, archaeological excavations revealed three sacred buildings
145 (two Orthodox and one Catholic churches), numerous profane buildings (some of which are
146 monumental in scale), and numerous and varied movable archaeological finds. All these data indicate
147 that during the last decades of the 13th to the middle of the 15th century, Rudnik was an important
148 developing settlement composed of native and newcomer populations of different social and religious
149 characters(27).

150 Animal remains analyzed so far come from two Rudnik sites of Stacionar and Imanje Nikić. They
151 were collected from cultural layers dated to the period between the 14th and the first half of the 15th
152 century based on the findings of coins and pottery fragments. The Rudnik faunal assemblage
153 comprises the remains of mammals, birds, fish, and molluscs, of which 449 specimens were identified
154 to a species or at least a genus level. Most of the animal remains belonged to the domestic animals.

155 Caprines (sheep and goats taken together) are the most abundant taxa, followed by domestic cattle and
156 domestic pigs. Other mammal remains were of horse, dog, cat, roe deer, red deer, hare, and squirrel.
157 A small number of fish remains (common carp and sturgeon) and Jacob's scallop shell fragment were
158 also present. Domestic chicken was the only bird species identified and is represented with 20 (4% of
159 the total assemblage) bone fragments(28). The specimen OL1008 (a coracoid bone) was found within
160 the cultural layer inside of an economic/residential building at the site of Imanje Nikić.

161 **5. Fishbourne** (Roman BC50-AD280; OL1128; contact: Robert Symmons).
162 Discovered in 1960, Fishbourne Roman Palace is situated approximately 2.5km west of the city of
163 Chichester, near the south coast of Britain. The palace itself is the largest domestic Roman building
164 yet found north of the Alps, and today is a visitor center and museum displaying artifacts from the site
165 and 16 *in situ* mosaics. The site seemingly was occupied from the late Iron Age. Following the
166 Roman invasion of 43 CE, the area was used as a military supply base. This later evolved into a
167 “proto palace”, which included a large and luxurious bath house. Around 75 CE the proto palace was
168 enlarged into the “Flavian palace”: a massive high-status complex comprising 4 wings arranged in a
169 square around a formal garden with an informal garden to the south, leading down to nearby
170 Chichester Harbour. The footprint of the building is approximately 21,000 square meters, although
171 little is known about any ancillary structures that would undoubtedly have serviced the main complex.
172 From the second century the building experienced a gradual period of decline and contraction before
173 it was destroyed by fire in 280 CE.

174
175 Sample OL1128 was recovered in 2002, during excavations approximately 30 m east of the northeast
176 corner of the Flavian palace (site code FBE02, context 1040, catalog number CHCFB :
177 FBE02/CB88). The context was interpreted as a midden and dated to the mid-late first century.

178

179

180 **6. Vienna Avar Cemetery**, Austria (7th / 8th century; OL1231; contact: Henriette Baron).

181 The Avar Cemetery at Vienna Csokorgasse was excavated under the direction of Ludwig Streinz and
182 on behalf of the Historical Museum Vienna (today Wien Museum) in the years 1976 and 1976 within
183 the scope of a building project. In the course of the excavation, 705 burials were unearthed and
184 documented and the cemetery was excavated completely. According to Falko Daim and Ludwig
185 Streinz, the cemetery was continuously used: the first burials in the northeast date to the Early Avar
186 Period II (2nd quarter 7th century CE) and the last graves in the west and south of the burial area stem
187 from the Late Avar Period II to III (2nd and 3rd third 8th century CE). The burial type – inhumation
188 burials orientated west-east, displaying a variety of partially gender-specific burial goods – conforms
189 to the usual customs of the Middle and Late Avar Periods. For the most recent discussion of the site
190 and its zooarchaeological findings, see(29).

191 In 491 (70 %) of the 705 burials animal bones were found. In most cases these were remains of
192 chickens (319 graves, 45 %) and of sheep or goats (313, 44 %). Bones of cattle (240 burials, 34 %)
193 and of pigs (84, 12 %) also occurred in many burials. The chicken was interred in different degrees of

194 skeletal completeness. Of the mentioned domestic mammals, primarily the thigh portion containing
195 the femur was selected as a burial good. The faunal material also comprises some birds (domestic or
196 greylag geese, Western jackdaw, Northern Goshawk, Eurasian skylark, a pigeon, white-tailed eagle,
197 smew, gray partridge, Eurasian woodcock, as well as some unidentified bird remains), and some fish
198 (pike, a wels catfish, and different cyprinids). Four outstanding rich Late Avar burials in the south of
199 the cemetery area (burials 650, 690, 692, and 693) contained harnessed horses in an age fit for riding
200 usage. In addition, three of these comprised complete skeletons of fully grown large male dogs. From
201 the fourth equestrian burial (692) only a single dog tibia was recovered. Furthermore, a partial
202 skeleton of a young puppy was found in the digging shaft of burial 650. Another one was recovered
203 from a Middle Avar period child burial (burial 462). The equestrian graves contained grown up men
204 with belt fittings and in one case (burial 690) two children and an adolescent, the latter presumably
205 also with belt fittings.

206
207 7. **Kazan City**, Russia (16th-17th century; OL1584; contact: Dilyara Shaymuratova).

208 Kazan City is located in the Republic of Tatarstan in the east of the European part of Russia
209 (55°47'26" N 49°07'19" E), excavations were carried out on the territory of the modern backyard of
210 the Kazan Federal University in 2002. Sample OL1584 was located in layers from the "Early Russian
211 period" (16th-17th centuries). The study of the remains of bird bones was carried out by Igor Askeyev
212 and Dilyara Shaymuratova.

213
214 8. **Cheboksary City**, Russia (16th-18th century; OL1585; contact: Dilyara Shaymuratova).

215 Cheboksary City is situated in the Republic of Chuvashia in the east of the European part of Russia
216 (56°09'07" N 47°14'48" E), research and excavations of this archaeological site were carried out in
217 2004-2005 near the territory of the Vvedensky Cathedral. Sample OL1585 was located in layers of the
218 16th-18th centuries. Archaeozoological material was studied by Igor Askeyev and Dilyara
219 Shaymuratova.

220
221 9. **Elabuga hillfort**, Russia (17th-18th century; OL1599; contact: Dilyara Shaymuratova).

222 Elabuga hillfort is located in the Republic of Tatarstan in the east of the European part of Russia
223 (55°44'48" N 52°01'57" E), excavations were carried out on the territory of the location called
224 "Chertovo gorodishche" in 2003. Sample OL1599 was located in layers from the "Russian period"
225 (17th-18th centuries). Research of bone remains of birds was carried out by Igor Askeyev and Dilyara
226 Shaymuratova.

227
228 10. **Andlau**, France (10th-12th century; OL1934; contact: Olivier Putelat).

229 The village of Andlau (France, Bas-Rhin) is located in Alsace, about forty kilometers southwest of
230 Strasbourg. An archaeological excavation was carried out in 2008 by the PAIR/Archéologie Alsace,
231 at the "12 Cour de l'Abbaye", on an area of 900 m², under the direction of A. Koziol. It concerned the
232 gardens, located about thirty meters south of the Roman abbey church, in the center of the current
233 village. This operation constitutes the first archaeological approach of the medieval abbey, which
234 until then was known only from written sources. The latter indicates that this Benedictine monastery,
235 reserved for women from the aristocracy, was founded in 879/880, by Richarde, the wife of the
236 emperor *Charles le Gros*. The excavation yielded more than 7300 bone remains, 4304 of which are
237 dated to phase A2 of the site (10th-12th century CE), from which the OL 1936 sample originated. Of
238 these 4304, 2108 were determined, the 85 chicken bones accounting for 4% of the NISP. It should be
239 noted that the examination of some of the sieve refusals yielded several thousand fragments of
240 eggshells, mainly attributable to the hen, as well as the discovery of a dwarf hen(30).

241
242

243 11. **Studenica Monastery**, Serbia (14th-15th century; OL1214; contacts: Nemanja Marković and
244 Jelena Bulatović).

245 The Studenica Monastery is located on a flat plateau in the valley of the Studenica River, 49 km
246 southwest of Kraljevo in southwestern Serbia (approx. 220 km from Belgrade; 43°29'11.4"N
247 20°31'54.9"E). It represents one of the largest and richest medieval Orthodox monasteries in the
248 country which has been on the UNESCO list of the world cultural heritage since 1986. It was founded
249 at the end of the 12th century as an endowment and burial place of the progenitor of the Serbian
250 medieval ruling dynasty of Nemanjić, the Grand Prince (*Veliki Župan*) Stefan Nemanja (1166–1196,
251 †1199). Within its unique circular walls, the monastery complex contains: the Church of the Virgin
252 Mary (the central sacred building), the King's Church, as well as the churches of St. John and St.
253 Nicholas, several smaller sacred buildings, residential and economic facilities. Archaeological
254 excavations (with minor and major interruptions) were conducted between 1949–2014. The study of
255 everyday life in the medieval Studenica was part of the systematic archaeological research carried out
256 in two phases between 1989–1998 and 2010–2014. Several waste areas were discovered inside the
257 monastery complex and along the outer side of the southeastern rampart in the immediate vicinity of
258 the eastern gate(31). These waste areas contained a large amount of animal remains whose analysis
259 provided the first insights into the strategies of animal exploitation in one Orthodox medieval
260 monastery(32).

261 Faunal remains originated from midden areas both outside and inside the monastery walls. Based on
262 the stratigraphic data, coins and ceramic fragments findings, these middens with faunal remains were
263 dated to the period from the beginning of the 14th till the middle of the 15th century. Out of the total
264 number of identified specimens (NISP=1949), 1527 belonged to mammals, 282 to birds, and 140 to
265 fish. The majority of mammal remains (92%) were from economically important domesticates: sheep,
266 goat, pig, and in a smaller number cattle. Hare is the best represented game species, whereas only one
267 red deer tine fragment was found(32). The diversity of fish species and written sources (f.e.,

268 Studenica Typikon) point to the fact that the exploitation of fresh fish had an important place in the
269 medieval economy of the monastery. Besides the remains of the fish available more or less locally
270 (such as Wels catfish, carp, and pike), remains of migratory sturgeons (such as beluga, Russian
271 sturgeon, and stellate sturgeon) which were probably transported from the Danube area about 200 km
272 far from the monastery, were found too(33).

273 Bird remains were found in three of the four analyzed midden areas. Out of 282 bird remains, 243
274 were determined to a species level. Remains of the five species were identified: chicken, duck, goose,
275 pigeon, and eagle. Remains of chicken are the most frequent and comprise 227 specimens (i.e., 93.5%
276 of the total bird remains identified to the species level). Chicken age and sex profiles shows that older
277 hens were the most numerous in all midden areas implying that they were exploited primarily for the
278 egg production(34). The sample OL1214 (a coracoid) was recovered in the midden area formed on the
279 Buildings V and VII ruins inside the monastery walls and dated to the last decade of the 14th century
280 and the first decades of the 15th century.

281 12. **Naderi Tepe**, Iran (19th century; OL2267, OL2268, OL2272; contact: Marjan Mashkour).
282 Three samples:

- 283 a. Tepe Naderi 2018 - Tr1, S2, F5, A12. DNA ID: OL2267
- 284 b. Tepe Naderi 2016 - Tr1, S2, F5, 34. Depth 290cm. DNA ID: OL2268
- 285 c. Tepe Naderi 2016 - Tr1, S2, F5, A41. Depth 330cm. DNA ID: OL2272

286

287 Tepe Naderi is a 20m high artificial mound with a long occupational sequence that lasted from the
288 late Chalcolithic/early Bronze Age through the early Iron Age (5128-158BP to 2752-27BP;
289 Achaemenid to Sassanid period), a short medieval age settlement from 10th-11th Century CE, and
290 eventually an occupational phase from Qajar period (18th-19th Century), when a fortress was built at
291 the top of the mound overlooking a lower town which was a fortified enclosure.

292

293 F5 is a bag-shaped pit dug into the medieval layers at the foot of the Tepe in the lower town. The pit
294 is 1.16m at the opening and 2.96m at the bottom (2.48m deep) in the south of Trench 1, from which
295 dozens of fragments of blue-white stonepaste wares and many bone fragments were discovered. The
296 pit was found and partly emptied during the first campaign in 2016 and partly in 2018. Therefore, it is
297 plausible that samples from 2016 and 2018 are from the same individual. All samples are from the
298 same context.

299

300 At first, since the pit cuts through the medieval layers in the lower town at the foot of the tepe, it was
301 attributed to the medieval period. However, this was later revised based on a finer study on the
302 material and some radiometric dating. A calibrated radiocarbon date of a piece of animal bone places
303 the pit within the range of 146-145 BP, which falls in the Qajar period. Two thermoluminescence
304 dates of two pottery samples are 180-250 and 150-210 BP, or between 1700 and 1800 CE, which are
305 consistent with the radiocarbon-dated animal bone.

306

307 Further radiocarbon dating conducted in the present study corroborates the previous dating. The
308 calibrated age range and associated probabilities for sample OL2272 is: 1698-1723 (23.6%); 1814-
309 1835 (20.8%); 1885-1910 (23.8%). See section below for full description of radiocarbon dates
310 obtained in the present study.

311
312 13. **Bard-e Mar** (Bem), Kurdistan (18th-early 21st century; OL2178; contact: Amir Saed
313 Mucheshi and Marjan Mashkour).

314
315 Bard-e Mar is situated in the Zargos region (35°9'39.63" N, 46°22'14.35" E, 790 m above sea level),
316 on an old terrace of the Sirwan River in Sarvabad County, (a part of the Hawraman region), in the
317 Kurdistan Province, Western Iran. Bard-e Mar is a small site of approximately two hectares with a
318 steep slope towards the river. Bard-e Mar was recorded during the Darian Dam Archaeological
319 Salvage Project (DDASP) directed by Fereidoun Biglari in 2014 and excavated by Amir Saed
320 Mucheshi in 2015. Excavations at Bard-e Mar were conducted in two trenches, named Trench I and
321 Trench II, both reaching the virgin soil. The cultural finds included potsherds, ground stones, clay
322 pipes, rich faunal remains and rectangular and circular stone architectural structures. The Hawraman
323 region has had a traditional and special masonry architectural style due to steep slopes of the
324 mountains, and its continuity to the modern day is observable in evidence from Bard-e Mar. It is
325 worthy to note that the diagnostic glazed pottery vessels were not discovered at site. As a result of
326 relative and absolute chronological comparisons, two distinct periods were identified in Bard-e Mar,
327 including the Middle Islamic (13th to 14th century A.D.) and the Late Islamic, the reign of Qajar
328 Dynasty (18th to early-20th century A.D.). The finds from the Middle Islamic layers are less than its
329 upper part, due to the reduction of the dimension of the trenches. The data from the Middle Islamic
330 period are comparable to the western regions of Iran. The Qajar Dynasty/Late Islamic finds,
331 especially clay pipes, are comparable with the Late Ottoman period in the Iraqi Kurdistan and Kurdish
332 potteries reported from the Zagros region in the Late Islamic period(35).

333 Faunal remains were studied by H. Davoudi, R. Khazaeli and M. Mashkour in the National Museum
334 of Iran and Bioarchaeology Laboratory, Central Laboratory of the University of Tehran. A total of
335 2807 pieces of animal bones have been discovered from excavations in Bard-e Mar, of which 1718
336 samples belong to Trench I and 1089 pieces belong to Trench II. The bones are generally placed in
337 the group mammals and birds, and only one piece of fish bone was identified in the collection. Cattle,
338 sheep and goats are dominant, comprising 50% of the collection. A small amount of the collection
339 derives from wild sheep and goats, deer, equines, foxes, forest otters and rabbits. A significant part of
340 animal remains from the Late Islamic period belong to birds, of which some are domestic chickens
341 and their relatives. Examining the animal remains of Bard-e Mar shows that its subsistence economy
342 is based on animal husbandry and the people living in this area used goats, sheep and cattle as the
343 main source of livelihood, a method that is still common in this region(36).

344 In this paper, Sample OL2178 was analyzed, which belonged to the right femur of *Gallus gallus*,
345 derived from Trench I, Locus 14, Code a#56, the Qajar Dynasty/Late Islamic period (18th to early 20th
346 century A.D.).

347 Description of bird used as positive control

348 To validate the shotgun sequencing and baiting procedure, we also processed DNA from a modern
349 bird displaying symptoms of Marek's Disease from a naturally acquired infection. A feather from the
350 bird, a Silkie chicken, was provided by Gabrielle Franklin of the Silkie Club of Great Britain. At the
351 time of infection, the bird was unvaccinated and 3-4 years of age. Symptoms included a sudden loss
352 of weight and dropped wing/paralysis on the left side. Following the development of these more
353 severe symptoms, the bird was euthanized to prevent suffering.

354 Radiocarbon dating

355 In total, four samples were radiocarbon dated ([Table S10](#)) using either the Oxford Research
356 Laboratory for Archaeology and the History of Art or Beta Analytic. Uncalibrated dates were
357 calibrated using IntCal20: Northern Hemisphere(37). In all cases, there was a degree of ambiguity in
358 the measured sample ages, so raw plots are given below ([Fig. S8](#)).

359 Ancient DNA extraction

360 DNA extractions were performed in dedicated ancient DNA (aDNA) facilities at the PalaeoBARN
361 (University of Oxford). DNA was extracted from chicken bone samples ([Table S1](#)) in a dedicated
362 ancient DNA laboratory using the appropriate sterile techniques and equipment. Prior to grinding,
363 ~0.5mm of the exterior surface of the bone was removed using a Dremel 3000 electric hand-drill.
364 Extraction was carried out using the Dabney extraction protocol(38).

365 Library preparation and preliminary sequencing

366 Illumina libraries were built following either the protocol in(39) or(40), but with the addition of a six
367 base-pair barcode added to the IS1_adapter.P5 and IS3_adapter. P5+P7 adapter pair. The libraries
368 were then amplified on an Applied Biosystems StepOnePlus Real-Time PCR system to check that
369 library building was successful, and to determine the minimum number of cycles to use during the
370 indexing amplification PCR reaction. A six base-pair barcode was used during the indexing
371 amplification reaction resulting in each library being double-barcoded with an "internal adapter"
372 directly adjacent to the ancient DNA strand and which would be the first bases sequenced, and a
373 traditional external barcode that would be sequenced during Illumina barcode sequencing. An
374 additional sequencing library was built for sample OL1385, which had two external 6 bp indices
375 appended to the P5 and P7 Illumina sequencing primers, and had no internal index tag. Up to 200
376 libraries with unique barcode combinations were pooled at equimolar levels (as determined by an
377 Agilent Technologies 2200 TapeStation) and an 80 - 150 bp run was carried out on an Illumina HiSeq
378 2500/4000/X sequencer at Novogene or Macrogen.

379 Preliminary analyses of sequencing data using HAYSTAC

380 We screened 995 ancient chicken (*Gallus gallus domesticus*) DNA libraries, with HAYSTAC(6), with
381 default settings, for the Gallid Alphaherpesvirus 2 (MDV) genome, using a custom database of
382 complete herpesvirus genomes obtained from in the NCBI RefSeq database (Table S11). This analysis
383 identified 18 samples with at least one MDV read (range: 1–785; [Table S2](#)). To ensure the validity of
384 the positive identifications in samples with a higher number of confidently assigned MDV reads
385 (>50), we ensured that the respective evenness of coverage ratio (genome coverage / fraction of
386 genome covered) was less than 10, and that appropriate chemical damage patterns characteristic of
387 ancient DNA were identified ((41); [Fig. S2](#)). These 18 samples, as well as a modern sample with MD
388 symptoms (OL1099; positive control) and a sample for which we did not identify any MDV reads
389 (OL1214; negative control) were subsequently genome captured (see below).

390 Design of probes for in-solution capture

391 Custom DNA probes for a tiled baiting approach were designed and synthesized by Arbor
392 BioScience, based on the *Gallid alphaherpesvirus 2* genome (strain RB-1B; accession EF523390.1,
393 NCBI). Baits were only constructed for one copy of each of the two terminal repeats (coordinates 1-
394 14004 and 165217-178246 in EF523390.1 were excluded), and regions of low complexity in the
395 genome were masked . Oligonucleotide baits were designed approximately every 28 nucleotides,
396 yielding 8403 50-mer probe sequences for the whole MDV target genome. The probes allowed for the
397 hybridisation of both modern and ancient strains of MDV, while limiting carryover of endogenous
398 DNA.

399 In-solution capture and sequencing of captured libraries

400 Additional libraries were either amplified or re-built from extracts of the samples that were selected
401 for targeted genome enrichment ([Table S2](#)), following the metagenomic screening for MDV DNA
402 reads. These selected libraries were amplified again following the same indexing and PCR
403 amplification strategies as previously described, and were condensed in a final volume of 25 µl.
404 Libraries from samples OL1008, OL1128, OL1214, OL1231, OL1385, OL1585, OL1987, OL1999
405 were built once and were also amplified and captured once, whereas for samples OL1389, OL1584,
406 OL1599, OL1934, OL1936, OL1984, OL1986, OL2178, OL2267, OL2268, OL2272 three different
407 libraries were built from the same extract and each library was subsequently amplified and captured
408 ([Table S2](#)). Any additional libraries built for the samples that were captured more than once, were
409 indexed and amplified for sequencing, using conventional full-length P7 and P5 Illumina primers that
410 were both indexed with external 6 bp indices, instead of having one internal and one external
411 index(40).

412 MDV genome capture and paired-end sequencing on Illumina NovaSeq lanes were performed by
413 Arbor BioScience. Specifically ~200 million 150 bp paired-end reads were generated per capture
414 sequencing pool. As a positive control, one modern chicken feather sample (OL1099) which
415 displayed symptoms characteristic of MD was also processed using the above procedure and yielded a

416 4× genome. Sample OL1214 yielded no MDV-specific reads following screening and was included as
417 a negative control in the genome capture protocol.

418 MDV-positive samples

419 In total, we performed genome captures for 20 samples, comprising a modern positive control
420 (OL1099), an ancient negative control (OL1214) and 18 ancient samples with varying degrees of
421 MDV positivity (Table S2). Of these, 16 samples (including the positive control) were unambiguously
422 positive for MDV DNA. The negative control was enriched to 451 post-capture reads, but a majority
423 of these were short (<25bp) and therefore likely nonspecific (Table S2). Three further samples
424 (OL1008, OL1231 and OL1128) yielded very few (<60) post-capture reads, and these were
425 overwhelmingly short (<25bp), so were considered negative for MDV (Table S2).

426 Capture efficiency

428
429 For MDV-positive samples, enrichment for MDV sequence ranged from 1.65 to 273.12-fold increase
430 in unique DNA templates, allowing us to increase the depth of coverage of the ancient MDV isolates
431 (range: 0.13 - 41.92), reduce the percentage of missing sequence data and reconstruct consensus
432 genomes (Table S2). The genome enrichment captured virtually all the unique DNA templates that
433 were available in the analyzed libraries, as shown by the high percentage of duplicated reads post
434 capture (range: 56.6 - 99.98%; Fig. S1, Table S2).

435 Short read alignment of ancient data

437 The captured data were aligned with the bwa aln algorithm against the RB-1B (EF523390.1) MDV
438 reference genome with default parameters apart from disabling the seed option (“-l 1024”) (42).
439 Because the MDV genome has terminal long (TRL) and short (TRS) repeat regions (14kbp and
440 13kbp, respectively), one repeat from each of these duplicated regions was masked (coordinates 1-
441 14004 and 165217-178246 in EF523390.1) in order to avoid low mapping quality stemming from a
442 DNA read aligning to multiple positions, and to retain the maximum number of reads.

443 Testing read sharing between chicken and MDV

444 To detect sequence homology between chicken and MDV genomes that could lead to false positive
445 identification of ancient MDV-positive samples, we simulated short read sequencing data based on
446 the RB-1B (EF523390.1) genome and mapped these regions against the chicken genome (GRCg7b).
447 To simulate reads, ART was used (art_illumina -ss HS10 -i [input_fasta] -l 100 -f 50 -p -m 350 -s 50 -
448 o [output_fastq]). Reads were then mapped against the chicken genome using the bwa aln algorithm.

449 Genotyping of ancient data

450 Aligned reads had 5 base pairs trimmed from both their 5' and 3' ends with bamUtil v 1.0.14(43), and
451 read group identifiers were added to the resulting bam files by using picard tools v 2.16.0(44).

452 The GATK package(45) was used for variant calling and sample genotyping. HaplotypeCaller v
453 4.1.2.0 was employed for SNP (single nucleotide polymorphism) calling with the following
454 parameters: the EF523390.1 MDV genome (masked for TRL and TRS; see above) was used as
455 reference, a value of 30 for the minimum base quality (Q) was required, all sites were outputted in
456 GVCF files, ploidy was set to 1, and physical phasing was not allowed (gatk HaplotypeCaller --
457 reference EF523390.1_mask.fasta --min-base-quality-score 30 --output-mode EMIT_ALL_SITES --
458 sample-ploidy 1 -ERC GVCF --do-not-run-physical-phasing true).

459 The GVCF files, from each individual sample, were aggregated into one with the CombineGVCFs v
460 4.1.2.0 tool. The aggregated data were input into GenotypeGVCFs for joint genotyping of the
461 different samples. The raw variants were further filtered using VariantFiltration, filtering in variants
462 with a minimum base quality (Q) value of 30 and a minimum sequence depth of 5 reads (gatk
463 VariantFiltration --filter-expression "QUAL >= 30.0 && DP >= 5"). VariantsToTable was
464 subsequently employed to convert the resulting VCF files containing the filtered SNPs to tables
465 (Table S12).

466 Generating fasta files

467 Consensus fasta files were also obtained from aligned reads in bam format using the htsbox pileup
468 tool (<https://github.com/lh3/htsbox>). The following parameters were used: a minimum read length of
469 25 base pairs, 5 base pairs were trimmed from each end of an aligned read, a value of 30 for the
470 minimum base quality (Q) and for the minimum read alignment quality (q) was set, for polymorphic
471 sites the majority frequency allele was called, and a minimum sequence depth of 5 reads was also
472 required (htsbox pileup -l 25 -T 5 -q 30 -Q 30 -M -s 5).

473 Publicly available (modern) data

474
475 Raw Illumina sequencing reads for samples KU173115.1, KU173116.1, KU173117.1, KU173118.1,
476 KU173119.1 were downloaded from the SRA using fasterq-dump v 2.11.0
477 (<https://github.com/ncbi/sra-tools>), and raw reads for samples MF431493.1, MF431494.1,
478 MF431495.1, MF431496.1 were provided to us by Jakob Trimpert(7). Modern samples AF243438.1,
479 AY510475.1, DQ530348.1, EF523390.1, EU499381.1, FJ436096.1, FJ436097.1, JF742597.1,
480 JQ314003.1, JQ806361.1, JX844666.1, KU744555.1, KU744556.1, KU744557.1, KU744558.1,
481 KU744559.1, KU744560.1, KU744561.1, KX290013.1, KX290014.1, MG432697.1, did not have any
482 associated raw sequencing reads deposited on the SRA, so full genome sequences were downloaded
483 from NCBI's Nucleotide database using a custom biopython (v 1.79) script (25). Metadata associated
484 with modern MDV strains can be found in [Table S3](#).

485
486 For publically available sequenced MDV strains that have undergone serial passage under
487 experimental conditions, only the lowest passage number was retained for time-calibrated
488 phylogenetic analyses. Therefore the following accessions were excluded from our BEAST analysis

489 (but were included in maximum likelihood phylogenies): JQ806362.1 (passage 31), JQ809691.1
490 (passage 41), JQ809692.1 (passage 61), JQ820250.1 (passage 81), JQ836662.1 (passage 101),
491 KT833852.1 (passage 70), KX290015.1 (passage 75), KX290016.1 (passage 110). We also excluded
492 strains that were duplicated in the dataset (KT833851.1 and NC_002229.3, both Md5). We further
493 excluded accession AF147806.2, since it was isolated in 1964 and subsequently experimentally
494 passaged in cell culture at least 45 times before being sequenced(4). On a maximum-likelihood
495 phylogeny AF147806.2 falls on a long terminal branch and a root-to-tip divergence analysis further
496 showed that it is enriched for substitutions compared to contemporary strains (see Fig. S9A and C and
497 "Temporal signal" section below). Repeated passaging likely introduced mutations in this strain that
498 obfuscates the temporal signal and makes it unsuitable for time-calibrated phylogenetic analyses.
499 Accession MG518371.1 was also excluded from our BEAST dataset as it lay in a clade with a vaccine
500 strain and thus likely represented contamination.

501

502 Removing BAC sequences

503 MDV reference genomes with accession numbers KT833851.1, KT833852.1, and FJ436097.1 were
504 contaminated with sequences from BAC (bacterial artificial chromosome) cloning vectors. BAC
505 sequences were removed from these genomes with a custom biopython script, and their non-
506 contaminated respective genomes were outputted in fasta format.

507 Masking of the modern genomes

508 Since the consensus MDV sequences in the ancient viral dataset had one of each of the terminal
509 repeats (TRL and TRS) masked, we also masked the same terminal repeats in our modern viral
510 sequence dataset.

511 The modern MDV genomes, which were downloaded from the NCBI nucleotide database, (cleaned
512 from BAC contamination) were split into 500 bp fragments, with a 5 bp overlap between each k-mer,
513 using the pyfasta split v 0.5.2 tool (<https://github.com/brentp/pyfasta>). Each fragmented genome was
514 subsequently aligned against the masked EF523390.1 MDV genome using the bowtie2 algorithm v
515 2.4.4(46) with default settings. The resulting bam files for each modern MDV genome were sorted
516 and passed to htsbox pileup with default settings (htsbox pileup -l 25 -M), in order to build new
517 consensus fasta sequences that had the TRL and TRS repeats masked, as for the ancient MDV
518 sequence dataset. Two sets of consensus fasta sequences were built for the ancient samples, one set
519 with $\geq 1x$ and one with $\geq 5x$ coverage depth per site (htsbox pileup -l 25 -M -s 1/5).

520 For the modern samples for which sequencing reads were available, Bowtie2 v 2.4.4(46) with default
521 settings was used to align these short reads against the masked EF523390.1 MDV reference genome,
522 and consensus fasta sequences were built using htsbox (htsbox pileup -l 25 -T 3 -q 30 -Q 30 -M -s 5).

523 Sequencing depth for sample OL1385

524

525 To calculate per-base sequencing depth for the highest coverage sample (OL1385), samtools depth (v.
526 1.10) was used. To plot the sequencing depth (Fig. S10), a custom R script was used to plot the mean
527 depth across non-overlapping bins of 300bp (25).

528

529 Phylogenetic clustering analysis

530 The R package fastbaps v 1.0.4(47) was used to identify phylogenetic clusters within our MDV
531 dataset, using the baps algorithm to perform Bayesian hierarchical clustering(48), unconstrained by
532 any phylogenetic tree. The 35 ancient and modern genomes used in the BEAST analysis were used as
533 input for the lineage clustering analysis. The resulting lineages were compared and plotted side-by-
534 side with the Maximum Credibility Tree, produced by TreeAnnotator v 1.10.4 from the BEAST
535 software suite(49), using the R library ggtree v 3.2.0(50); [Fig. S11](#)).

536

537 Positive selection analysis

538

539 The same alignments used for the BEAST analysis were also analyzed for positive selection using
540 codeml implemented in PAML (v4.9;(13)). Open reading frames were sliced out of the genomic
541 alignment with reference to coordinates of the annotated RB-1B genome (accession EF523390.1).
542 Exons from multi-exonic genes were concatenated and ORFs on the reverse strand were reverse
543 complemented. For ORFs in the repeated regions, only the internal repeat was included in the
544 analysis, meaning ORFs MDV000.5–MDV006.6 and MDV097.3–MDV103 were excluded. The
545 branch-site test in PAML was used (model=2; NSsites=2; fix_omega=0/1; omega = 1), specifying the
546 modern MDV sequences as the ‘foreground’ lineage and the ancient MDV sequences as the
547 ‘background’ lineage. Pairs of log-likelihood values for each locus were used to perform a likelihood
548 ratio test ($2\Delta\ln L$) with d.f. = 1, then the final p-value calculated by dividing the original p-value by 2
549 (as described in the PAML manual). P-values were transformed using the Benjamini-Hochberg
550 procedure in R (v4.2.1;(14)). Of the 154 non-redundant loci included in the analysis, 49 genes showed
551 significant evidence (corrected $p < 0.05$) for positive selection in modern MDV with respect to ancient
552 MDV. Full PAML results are presented in [Table S7](#). Positive selection results were plotted on a
553 circular representation of the RB1B genome in Fig. 2 using Circos(51).

554

555 Maximum Likelihood trees and Multisequence Alignments

556 Maximum likelihood (ML) phylogenetic trees (Fig. S4) were built using RAxML v 8.2.9(52), and
557 Neighbour Joining (NJ) trees (Fig. S3) were constructed using seaview v4. The percentage of
558 unknown bases (Ns) was calculated for each genome with the seqtk comp tool v 1.2.95, and all
559 samples with at least 1% of the genome covered (1782 sites) were kept, in an effort to retain and
560 analyze the maximum number of ancient MDV genomes. In total 42 modern MDV genomes from
561 previous studies ([Table S3](#)) and 11 captured MDV genomes from the present study were included. We
562 used consensus fasta sequences built with htsbox for this analysis (see above - for the captured

563 samples one set was built with coverage depth of 1x and one set with 5x). Of the 11 captured genomes
564 that were included, 1 genome was from a modern sample (OL1099; sampled 2014) while the
565 remaining 10 were obtained from archeological samples from the 14th-20th century ([Table S1](#)).

566 RAxML was used to build an unrooted tree with the following parameters: a random seed value for
567 rapid bootstrapping, a parsimony-based starting tree, a GTRGAMMA substitution model, and 100
568 bootstrap runs (raxmlHPC-PTHREADS -f a -T 10 -x \$RANDOM -k -# 100 -p \$RANDOM -m
569 GTRGAMMA). Seaview was used to build an NJ tree using the Jukes-Cantor model, with 100
570 bootstrap runs.

571 Maximum likelihood tree based on transversions

572 A midpoint-rooted maximum likelihood tree based only on transversions (Fig. S5), was built using 4
573 ancient MDV genomes (each with at least 80% coverage at 5x), 1 modern positive control from the
574 current study, and 30 modern MDV genomes from public sources. All transition polymorphisms were
575 set to “N” (unknown base) using a custom biopython script (25). All monomorphic positions were
576 also removed using the snp-sites tool v 2.5.1(53). A phylogenetic tree was then constructed using the
577 Lewis correction method for ascertainment bias(54) along with the ASC_GTRGAMMA substitution
578 model (raxmlHPC-PTHREADS -f a -T 10 -x \$RANDOM -k -# 100 -p \$RANDOM -m
579 ASC_GTRGAMMA --asc-corr lewis)

580 Maximum likelihood tree rooted with Herpesvirus of Turkeys

581 To confirm the placement of the root in the tree based only on transversions we used genomic data
582 from a *Meleagrid herpesvirus 1* (HVT; accession: NC_002641.1) as an outgroup to build a rooted
583 maximum-likelihood tree (Fig. S6a). Mafft v 7.123(55) was used to align the sequences of the
584 outgroup to the MDV genomes (mafft --maxiterate 1000 --thread 5 --nwildcard). For the phylogenetic
585 analysis we filtered out positions that were missing in the HVT genome (either “N” or gaps) using a
586 custom biopython(56) script. We removed all the positions that were either monomorphic or unknown
587 throughout all the samples in the alignment by using the snp-sites tool v 2.5.1(53). A phylogenetic
588 tree was constructed using the Lewis correction method for ascertainment bias(54) along with the
589 GTRGAMMA substitution model (raxmlHPC-PTHREADS -f a -T 10 -x \$RANDOM -k -# 100 -p
590 \$RANDOM -m GTRGAMMA), .

591 Filtering overlapping open reading frames for BEAST analyses

592 To obtain divergence time with BEAST v 1.10.4 we removed overlapping open reading frames
593 (ORF) based on a bed file containing ORF coordinates for EF523390.1 using a custom biopython
594 script (25). Non-coding regions of EF523390.1 were also included, which resulted in a bed file that
595 contained non-overlapping ORF and non-coding regions. These regions were extracted from the
596 htsbox consensus fasta files for each of the ancient and modern genomes using the seqkit subseq tool

597 of the seqkit package v 0.12.1(57). ORFs that were found on the minus (-) strand were reverse
598 complemented with the seqtk seq tool v. 1.2.95(58).

599 Filtering for coverage for BEAST analyses

600 In order to maximize the information content of the sequence alignments provided to BEAST and
601 reduce the noise introduced by missing data in our ancient samples, we used a custom biopython
602 script to calculate the percentage of missing data within each genomic region included in the BEAST
603 analysis (see above). Only ORFs and intergenic regions with at least 10% of sites covered in all
604 individual sequences in the alignment (i.e. 100% coverage: no missing data) were retained. We then
605 concatenated the ORF and intergenic regions separately using the seqkit concat tool v. 0.12.1.

606 Temporal signal

607 To assess whether our data possess a temporal signal we first examined the correlation between root-
608 to-tip divergence (in substitutions/site) and sampling date, using maximum likelihood trees
609 constructed in RAxML v. 8.2.9(52). Sampling dates of ancient sequences were fixed to the means of
610 the C14 calibrated distributions and the maximum-likelihood trees were rooted based on the outgroup
611 analysis (Fig. S6a). A total of 36 MDV genomes were included in this analysis: 30 modern, 1 modern
612 extensively passaged strain (AF147806.2), 1 modern positive control from the present study
613 (OL1099), and 4 ancient captured genomes from the present study (OL1385, OL1389, OL1986,
614 OL2272). Four variations were used: (i) all strains (Fig. S9A), (ii) all strains except AF147806.2 (Fig.
615 S9B), (iii) all modern strains (Fig. S9C) and (iv) all modern strains except AF147806.2 (Fig. S9D).
616 This analysis confirmed that AF147806.2 (cell passaged strain) did not undergo clock-like evolution
617 and can be considered as an outlier.

618 We further used a Bayesian date randomization test(59–61) (DRT) to examine the strength of the
619 temporal signal, by permuting sampling dates among genomes and performing 100 replicate analyses.
620 For the analyses the same dataset (n = 35, excluding AF147806.2) and BEAST model as below were
621 used, using an uncorrelated lognormally distributed (UCLD) relaxed clock and fixing the sampling
622 dates of the ancient sequences to the means of the C14 calibrated distributions. Chains were run for 50
623 million steps and the parameter sampling frequency set at every 5,000 steps. This resulted in
624 ESS>200 for all parameters in all replicate analyses. The HPD intervals of the mean clock rates
625 compared to an analysis with unpermuted sampling dates is shown in Fig. S12.

626 Regressing the root-to-tip divergence against sampling date showed a strong positive correlation (Fig.
627 S9) and the Bayesian DRT further showed strong evidence for a temporal signal in our dataset (Fig.
628 S12).

629 Finally, we performed a Bayesian Evaluation of Temporal Signal (BETS (62)) to assess the effect of
630 age uncertainty of the ancient MDV samples on the temporal signal. Here we compared the BEAST
631 model described below (using the probability densities of the radiocarbon dates of ancient samples as

632 priors for their ages) to a model using only the mean radiocarbon ages and a model without sample
633 ages. We used generalized stepping stone sampling (GSS (63)), implemented in BEAST, to obtain log
634 marginal likelihood estimates (MLEs) of the different models. The results show that a model
635 including sample ages and date uncertainty (log MLE = -123231.16) is preferred over a model using
636 only mean radiocarbon ages (log MLE = 136774.82) and a model without sample ages (log MLE = -
637 136777.73).

638 BEAST analysis

639 The BEAST v 1.10.4(49) package was used for the divergence dating and molecular clock rate
640 estimation of the MDV phylogeny. A total of 35 MDV genomes were included in this analysis: 30
641 modern, 1 modern positive control from the present study (OL1099), and 4 ancient captured genomes
642 from the present study (OL1385, OL1389, OL1986, OL2272). Publically available sequenced MDV
643 strains that have undergone serial passage under experimental conditions or contaminated with
644 vaccine strains were excluded from this analysis (see "Publicly available (modern) data" section for
645 accessions). Tip dates were provided to BEAST for both the modern and archaeological samples
646 (Table S13). We used the probability density function of the radiocarbon date as prior for the tip dates
647 of the 4 ancient samples. To do so we used the empirical calibrated radiocarbon sampler (ECRS;(64)
648 as implemented in BEAST. We used the same prior for OL1385 (which was directly dated) and
649 OL1389 (not directly dated) as the bones from which these sequences were derived were from the
650 same archaeological context.

651 The concatenated ORF alignment was partitioned further into codon positions with a custom python
652 script (25). Each partitioned alignment along with the concatenated intergenic region alignment, was
653 used as input for BEAST. The tree topology was fixed to the topology of the outgroup-rooted
654 maximum likelihood tree (without the outgroup) constructed only from transversion polymorphisms.
655 An independent GTR+ $\Gamma_{4(65,66)}$ substitution model was used for each alignment position and a constant
656 size coalescent model was specified as a tree prior.

657 We used an uncorrelated lognormally distributed (UCLD) relaxed clock model(67). We ran 8 MCMC
658 chains of 300 million steps each, with the parameter and tree sampling frequencies set at every 10,000
659 steps. The BEAST parameter log files were inspected with Tracer to ensure that all chains converged
660 to the same posterior distribution. After discarding 10% as burn-in we combined the chains which
661 resulted in ESS>200 for all parameters. The 95% CI of the coefficient of variation estimated under the
662 UCLD model excluded 0 (median=0.524, 95% HPD 0.34-0.76) indicating that the MDV sequences in
663 this tree did not evolve under a strict clock. To compare the placement of the root and the topology of
664 the ancient samples, we also repeated the analysis, but without imposing any tree topology
665 constraints.

666 Pairwise divergence

667 Average pairwise divergence between ancient (OL1385) and modern sequences was computed using
668 the R (v. 4.2.1) Ape package(68) and a window size of 100 bp and step size 25 bp. This analysis used
669 the same genomic alignment used for other analyses in the study. Pairwise divergence was plotted on
670 Fig. 2 using Circos as described elsewhere.

671 Functional validation

672 In order to functionally test the transactivation ability of the Meq oncogene in ancient vs. modern
673 MDV strains, an *in vitro* study system was constructed. The full length coding sequence of Meq from
674 the highest coverage ancient sample (OL1385; Buda Castle, Hungary), along with Meq from modern
675 strains (RB1B and Md5), were codon optimized and purchased from Integrated DNA Technologies
676 (IDT; IA, USA) with a 3× FLAG sequence appended to the N-terminus (Table S9). Since Meq
677 preferentially forms a heterodimer with chicken c-Jun, the chicken c-Jun coding sequence was also
678 synthesized with the addition of a 3× FLAG sequence on the N-terminus (UniProtKB accession:
679 P18870.2). All Meq and c-Jun sequences were cloned into the mammalian expression vector pTarget
680 (accession: AY540613) using the NotI and XmaI sites. A reporter construct comprising a 773 bp
681 section of the Meq promoter (which contains the putative AP-1 binding site AGTCATGCATGACGT
682 bound by Meq itself) upstream of the firefly luciferase gene on the pGL3-Basic vector backbone was
683 a kind gift from Venugopal Nair (Pirbright Institute, UK). A further reporter construct to normalize
684 transfection efficiency – pRL-TK – comprises the *Renilla* firefly luciferase downstream of the
685 relatively weak constitutive HSV-thymidine kinase promoter and was purchased from Promega (UK).
686 All vectors underwent whole-plasmid sequencing (Plasmidsaurus) prior to their use experimentally to
687 validate sequence integrity.

688
689 The chicken embryonic fibroblast cell line DF-1 was maintained in high glucose Dulbecco's Modified
690 Eagle Medium with GlutaMAX (ThermoFisher, UK) and 10% fetal bovine serum (ThermoFisher,
691 UK) in a humidified incubator at 37 °C and 5 % CO₂. The day before transfection, cells were
692 passaged and seeded into 96-well tissue culture plates at a density of 2×10⁴ cells/well. Wells were
693 transfected with a Meq construct (240 ng), c-Jun (240 ng), Meq-pGL3 Basic reporter (200 ng) and
694 pRL-TK reporter (4 ng) using 1.92 µl TransIT-2020 transfection reagent (Mirus; WI, USA). Twenty-
695 four hours post transfection, cell supernatants were discarded and cells were washed in cold
696 phosphate-buffered saline. Additional cell lysates were also prepared for immunoblotting of FLAG-
697 tagged protein. Luciferase measurements were conducted using the Dual-Luciferase Reporter Assay
698 System (Promega). Briefly, cells were incubated with 20 µl passive lysis buffer at room temperature
699 for 15 minutes. In opaque white 96-well plates, the Dual-Luciferase assay was completed in a
700 GloMAX plate reader (Promega), programmed to inject 100 µl Luciferase Assay Reagent II, then
701 quench and read *Renilla* luciferase with 100 µl Stop & Glo Reagent, both with a 2-second delay and
702 10-second integration time.

703

704 Over several experiments, it became apparent that the *Renilla* reporter did not serve as an adequate
705 background control because *Renilla* luciferase varied considerably depending on whether Meq was

706 present. *Renilla* luciferase measurements were substantially higher in wells containing Meq,
707 suggesting that the TK promoter was being driven by the transactivation ability of Meq. The same
708 phenomenon has been reported with pRL-SV40 constructs previously(69, 70). As a consequence,
709 firefly luciferase values normalized to *Renilla* luciferase were artificially diminished in Meq-
710 containing wells. Instead of normalizing to *Renilla* luciferase, we present the raw firefly luciferase
711 measurements. We confirmed via immunoblotting that the expression of ancient Meq was comparable
712 to that of other Meq constructs.

713 **Supplementary Text**

714 Sequence analyses of Meq gene: extended description

715 Given that Meq is known to be a major determinant of MDV virulence, we elected to consider this
716 gene in more detail. Meq exerts transcriptional control on downstream targets via its C-terminal
717 transactivation domain. This domain is characterized by PPPP (tetraproline) repeats, and the number
718 of tetraproline repeats is inversely proportional to the virulence of the MDV strain(22). Standard Meq
719 is 339 aa in length, but length variants of Meq exist: long(l)-Meq is 398 aa due to a tandem
720 duplication in the transactivation domain; short(s)-Meq is 298 aa; very short(vs)-Meq is 247 aa(71).
721 We conducted an analysis of 413 standard-length Meq sequences (comprising four ancient sequences
722 and one modern sequence derived from the present study, and 408 modern sequences derived from
723 public databases), and found that all modern Meq sequences have between two and five tetraproline
724 repeats. However, all ancient sequences have an extra tetraproline repeat (totaling six) that has been
725 disrupted in the modern lineage ([Table S8](#)).

726 We reconstructed the phylogeny of all Meq sequences using the RAxML(52) tree builder in Geneious
727 (v. 2019.2.3) with 100 bootstrap replicates. For each of the sequences, we also determined which of
728 the tetraproline repeats had been disrupted and the causative mutation for any disruptions. This
729 information was plotted onto the Meq phylogeny using iTOL (v. 6.5.8;(72)) along with the internal
730 branches where each disruption is likely to have taken place ([Fig. S7](#)).

731 Close inspection of the tetraproline motifs revealed that each motif has been lost at multiple points
732 throughout MDV phylogeny, confirmed by the presence of independent disruptive mutations.
733 Moreover, there is evidence that the loss of tetraproline motifs is ordered. Following the loss of the 6th
734 tetraproline motif (which occurred in the common ancestor to all modern strains), the 4th tetraproline
735 motif is lost independently in two major lineages of European and Asian/N. American strains. Next,
736 the 2nd tetraproline motif is most commonly lost, followed by either the 5th or the 1st tetraproline
737 motif, usually in terminal branches of the tree. The selective pressure for the ordered loss of the 4th
738 then 2nd tetraproline appears to be particularly strong – in the major Asian/N. American lineage, the
739 2nd tetraproline was lost 6 independent times. Intense selection pressure within the 2nd and 4th
740 tetraproline motifs was also confirmed using a small number of Meq sequences derived from whole
741 genomes in the positive selection analysis described above (where codons 176 and 217 were under

742 selection in the 2nd and 4th tetraproline, respectively). Occasionally, the 3rd tetraproline is lost after the
743 6th tetraproline, but this typically occurs at terminal branches ([Fig. S7](#)).

744 The loss of tetraproline motifs appears to act as a ratchet, whereby each subsequent loss results in an
745 increase in virulence, and once lost, motifs cannot be regained. This results in a stepwise scaling of
746 the fitness landscape wherein the order of losses is important. Although there are some observations
747 of virus lineages exhibiting an alternative loss order, such lineages are not widespread, suggesting that
748 they may become stuck in local fitness peaks and are outcompeted by lineages following the order
749 described above.

750 Functional validation results: extended description

751 Having identified the crucial oncogene Meq as being positively selected between the ancient and
752 modern strains, we sought to test whether the polymorphisms translate into a change in Meq function.
753 Meq is a regulator of transcriptional activity, and the strength of the transcriptional activation of target
754 genes is strongly linked to virulence(73). In order to compare transcriptional activation between
755 ancient and modern MDV strains, the Meq gene was cloned based on the sequence from the highest
756 coverage ancient sample (OL1385; Buda Castle, Hungary) alongside Meq from three modern MDV
757 strains (RB1B and Md5, both very virulent pathotypes). Meq forms a functional heterodimer with a
758 chicken protein – c-Jun – which is required for transcriptional activation, and so chicken c-Jun was
759 cloned and expressed alongside each Meq construct in DF-1 cells. As a reporter of transcriptional
760 activity, the Meq promoter (which contains an AP-1 binding site) in an expression vector upstream of
761 the firefly luciferase gene was co-transfected with the Meq/c-Jun pair.

762
763 As anticipated, Meq from the modern very virulent strains of MDV (RB-1B and Md5) showed the
764 greatest transactivation ability, with RB-1B Meq exceeding a ten-fold enhancement of luciferase
765 signal compared to empty vector (**Fig. 3c**). As previously reported, we found that c-Jun is important
766 for Meq function, exemplified by RB1B Meq transactivation being severely abrogated without c-Jun
767 co-expression. There was, however, a small transactivation effect of RB1B Meq in isolation, possibly
768 as a result of endogenous c-Jun in DF-1 cells forming a small amount of functional heterodimer. Most
769 significantly, we found that the ancient Meq sequence derived from the ancient Hungarian strain of
770 MDV (OL1385), was a very weak transactivator. Transactivation from this construct was still
771 significantly elevated relative to baseline, but was considerably less than Meq from modern strains.
772 These findings support the hypothesis that ancient Meq, and thus ancient MDV, was considerably less
773 virulent than modern strains.

774 775 Choice of tree root: extended description

776 When running the BEAST analysis with a phylogenetically unconstrained tree, we found that BEAST
777 placed the root immediately prior to sample with the earliest tip date (Fig. S6b). This is expected as
778 BEAST has no specific mechanism to determine the root without inclusion of an outgroup. As a
779 result, a tree topology determined by BEAST showed the ancient samples in a paraphyletic group. In
780 contrast, when the tree topology was determined (using maximum likelihood) while including an

781 outgroup (herpesvirus of turkeys; HVT), the ancient samples fall into a well-supported monophyletic
782 clade (bootstrap: 94; Fig. S6a). Although a closely related virus, HVT is too divergent to have been
783 included in the BEAST analysis as an outgroup along with MDV samples. To ensure accurate root
784 placement, our BEAST analysis therefore used a tree that was constrained to the topology as
785 determined by the maximum likelihood analysis with HVT as an outgroup, but with the HVT
786 sequence removed.

787

788 BEAST results: extended description

789 The mean root age of the tree was estimated around 1602 CE, with the mean times of the most recent
790 common ancestors (tMRCA) for the Eurasian and North American modern lineages tracing back to
791 1903 and 1909 CE respectively. The mean UCLD clock rate was estimated to be $7.69E-6$
792 substitutions/site/year, an estimate that is in the same order of magnitude as other dsDNA viruses(74).
793 The posterior age distributions estimated for the ancient MDV samples OL1385 (1803), OL1389
794 (1802), OL1986 (1594) and OL2272 (1821) resembled the corresponding posterior density functions
795 of the radiocarbon dates (Fig. S8), which were used as empirical priors on the sample ages, showing
796 that the MCMC chain sufficiently integrated across the uncertainty in the ages of the ancient MDV
797 samples. One exception is OL1986; while there is some support from the radiocarbon dating for the
798 sample dating to before 1627 CE, there is little support from the BEAST results. Similarly, the
799 BEAST results show less support for OL1385 and OL1389 to be more recent than 1858 and 1871 CE,
800 respectively.

801

802 Phylogenetic clustering analysis: extended description

803 A total of 4 phylogenetic clusters were identified by fastbaps ([Fig. S11](#)). The first cluster included the
804 4 ancient samples with the highest genome coverage, followed by a Eurasian and a North American
805 cluster, and a cluster of modern samples of both Eurasian and North American origin. As the
806 clustering is performed without being constrained by the BEAST MCC tree, the identified
807 phylogenetic clusters further corroborate the presence of a monophyletic Eurasian and North
808 American lineages (as it can be observed in the topology estimated by BEAST) as well as the
809 presence of a “transitional” lineage between the two modern MDV lineages.

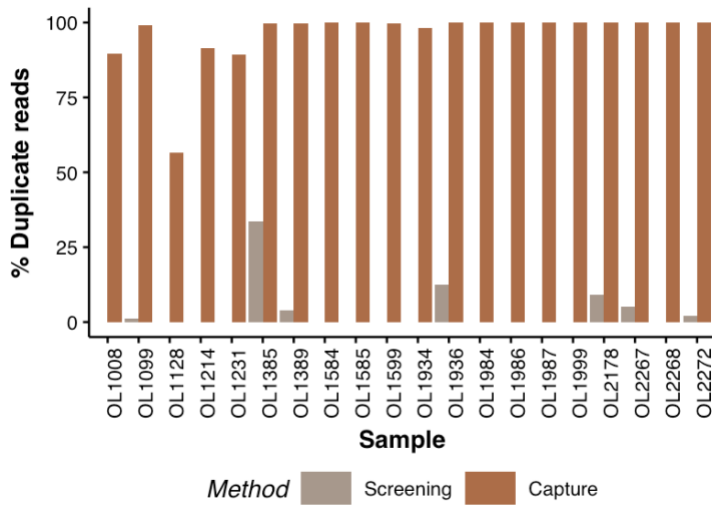
810

811 Read sharing between chicken and MDV: extended description

812 To test whether the chicken and MDV genomes share significant homology that could result in read
813 sharing between the host and virus, we simulated short-read data from the MDV genome and mapped
814 these against the chicken genome. We identified one region which shares significant homology
815 between the chicken and MDV and could be a source of read sharing: MDV001/MDV080 is a RNA
816 telomerase subunit (vTR), 435bp in length, that is presumed to be a recent gene capture from the
817 chicken genome. There was no evidence of significant read sharing between the chicken and MDV
818 genomes – depth of coverage in our highest coverage ancient sample (OL1385) over the homologous
819 region (coordinates: 141336-141771; depth: 58.8 ± 24.8) was in line with the wider region
820 (coordinates: 140000-142000; depth 77.0 ± 47.9).

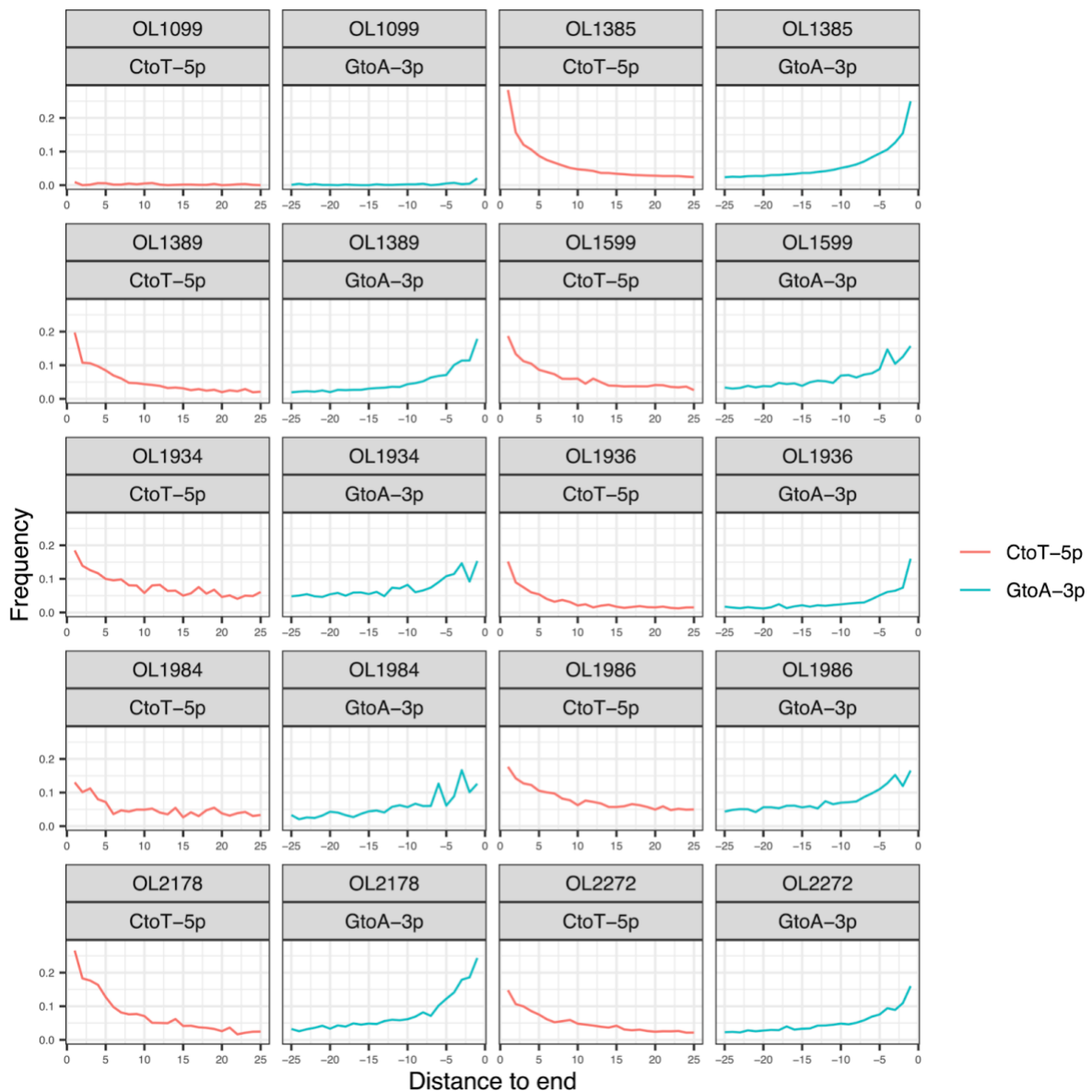
821 **Supplementary Figures**

822



823 **Fig. S1.**

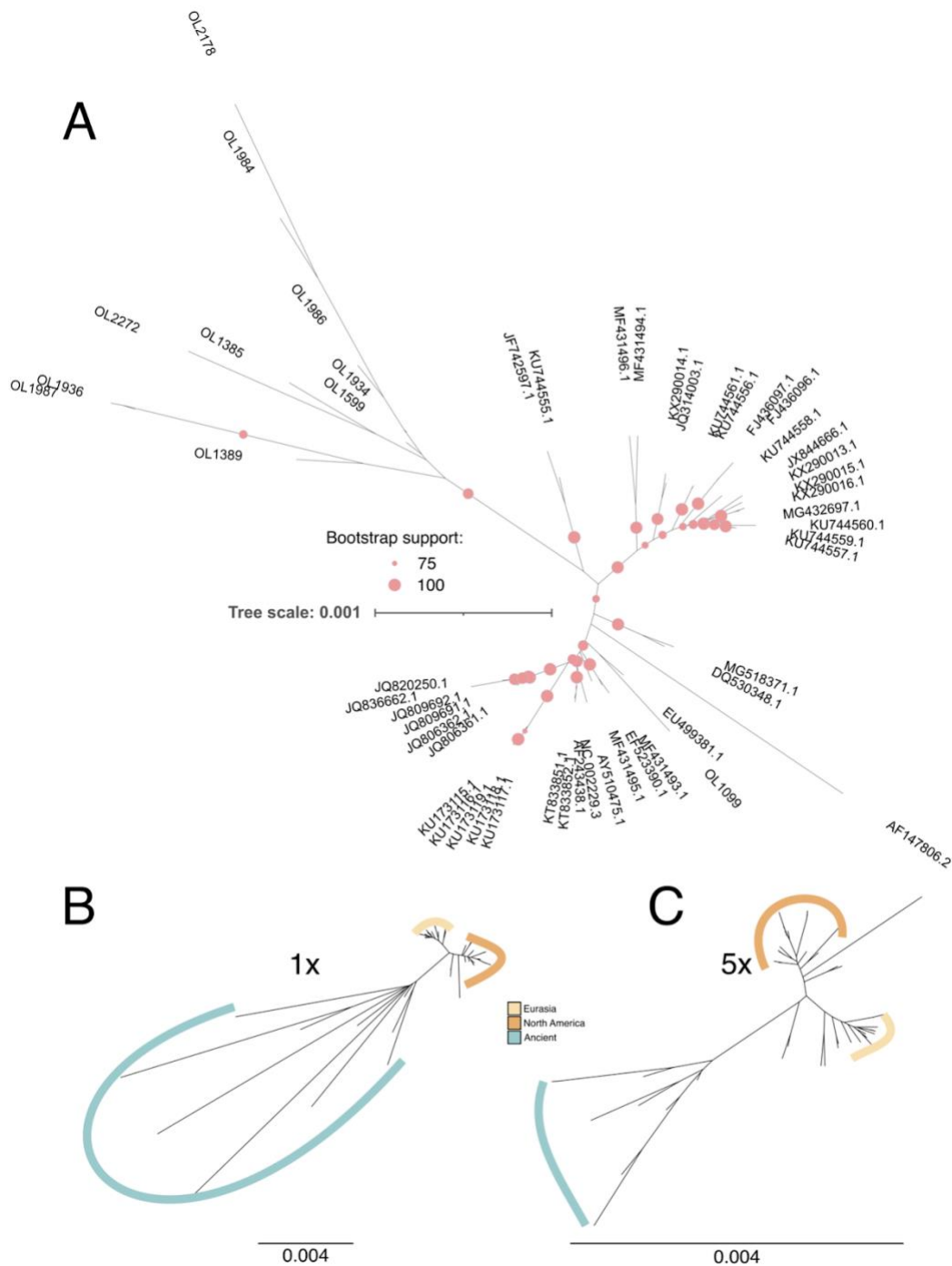
824 **Percentage of duplicated reads after sequencing of screening and bait-captured libraries.** In
825 most cases, baiting of the sample resulted in near-saturation of duplicated reads, meaning almost all
826 unique molecules in the sample were sequenced.



828

829 **Fig. S2.**

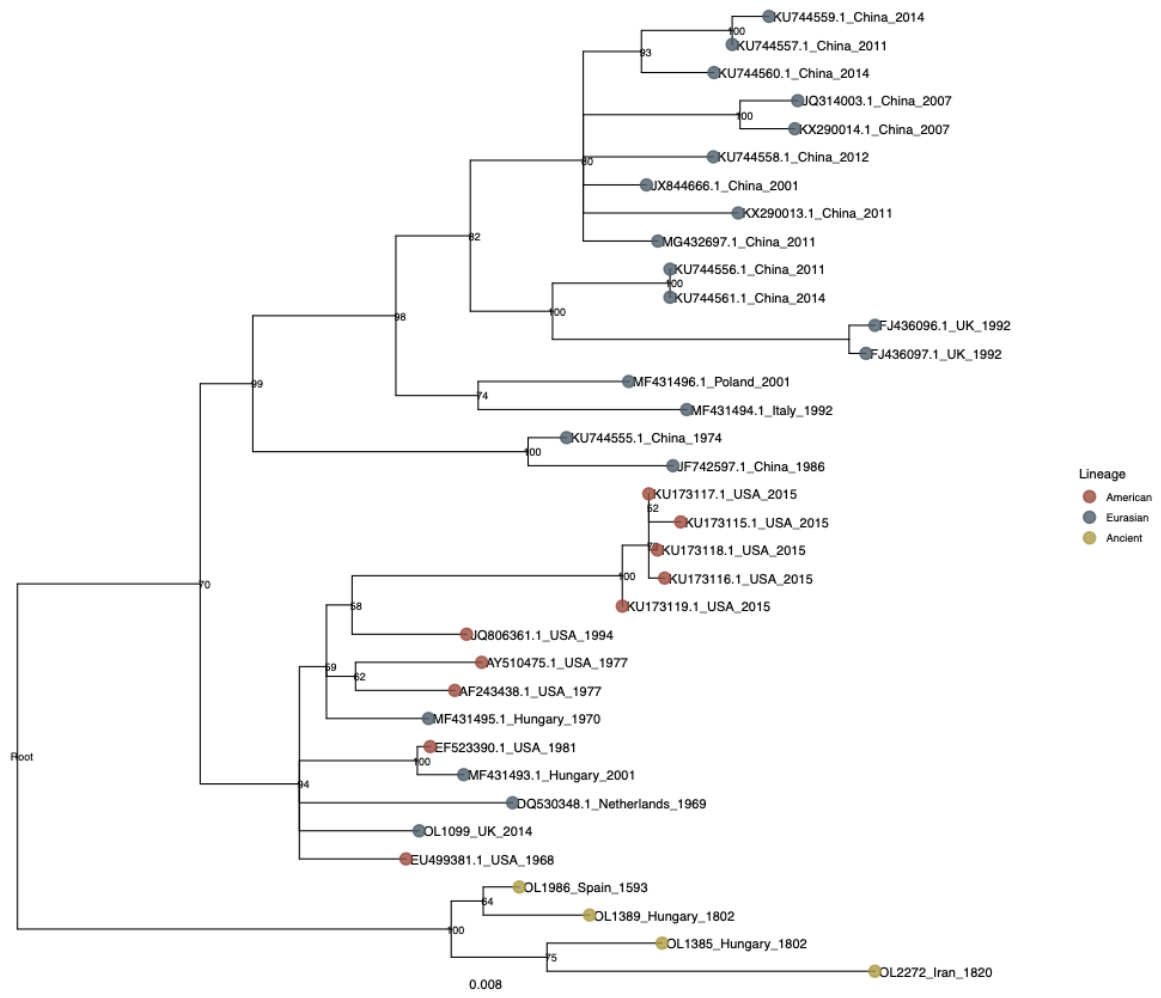
830 **DNA damage profiles of DNA derived from archaeological samples.** DNA reads from all samples
 831 with genomic coverage $>1x$ were analyzed using the MapDamage program(41) which assesses the
 832 rate of C-to-T and G-to-A transitions as a result of the spontaneous deamination of cytosine. As a
 833 control, reads from a modern sample (OL1099; 2014 CE) were also included.



834

835 **Fig. S3.**

836 **Neighbor-joining phylogenies of modern and ancient MDV genomes.** (A) Bootstraps of ≥ 75 are
 837 displayed as filled circles. Captured samples (with 'OL' prefix) from the present study were included
 838 if the genome had $\geq 1\%$ coverage at 5x. Differences in branch lengths for ancient samples are
 839 highlighted when using a depth of coverage threshold of 1x (B) and 5x (C).

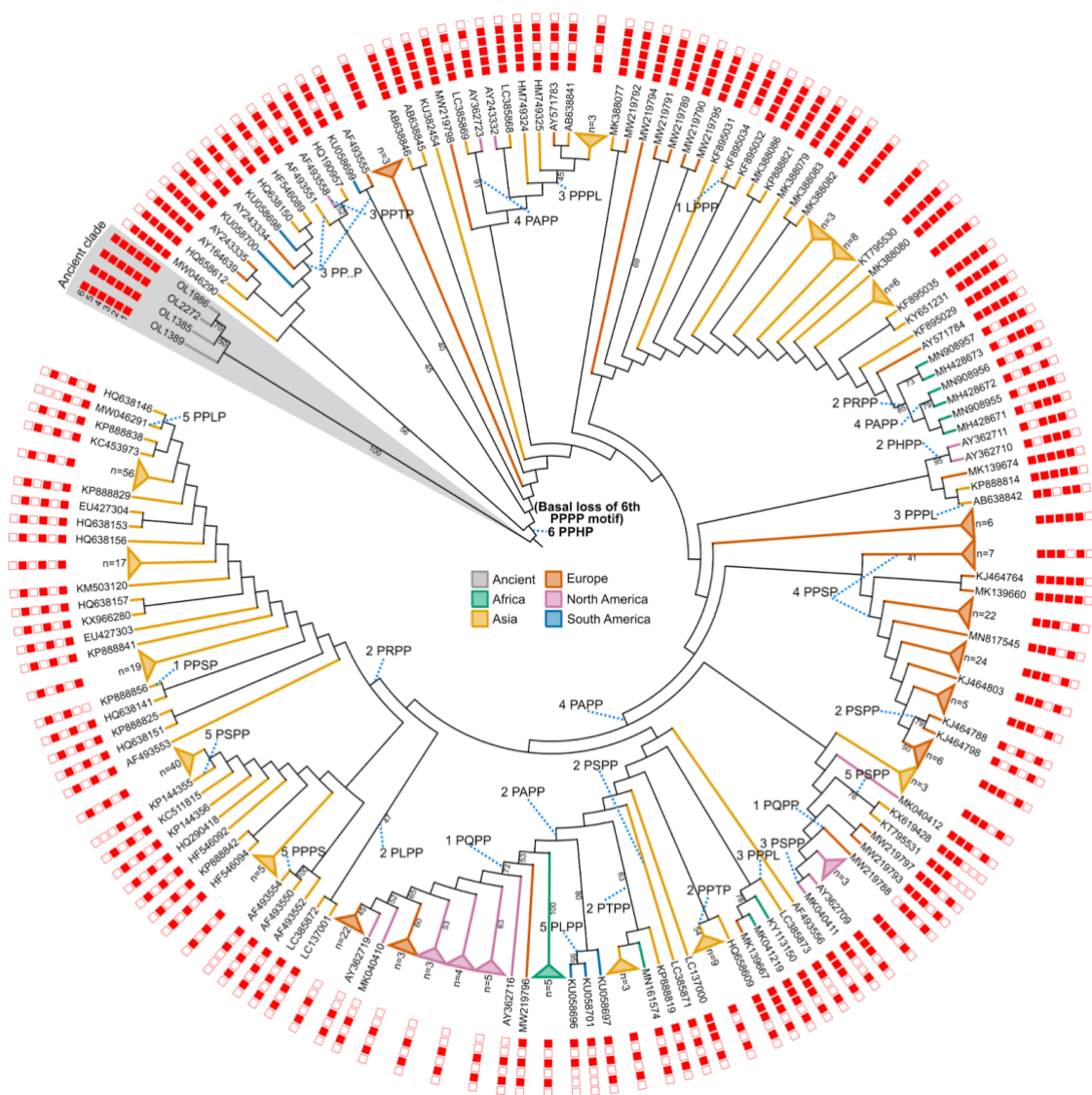


845

846 **Fig. S5.**

847 **Midpoint-rooted maximum likelihood tree using transversion SNPs only.** Tree was built using
 848 RAxML(52), with ascertainment correction for SNPs, and included all ancient samples with a
 849 genomic coverage of $\geq 20\%$. The placement of the root was confirmed using an outgroup (Fig. S6a).

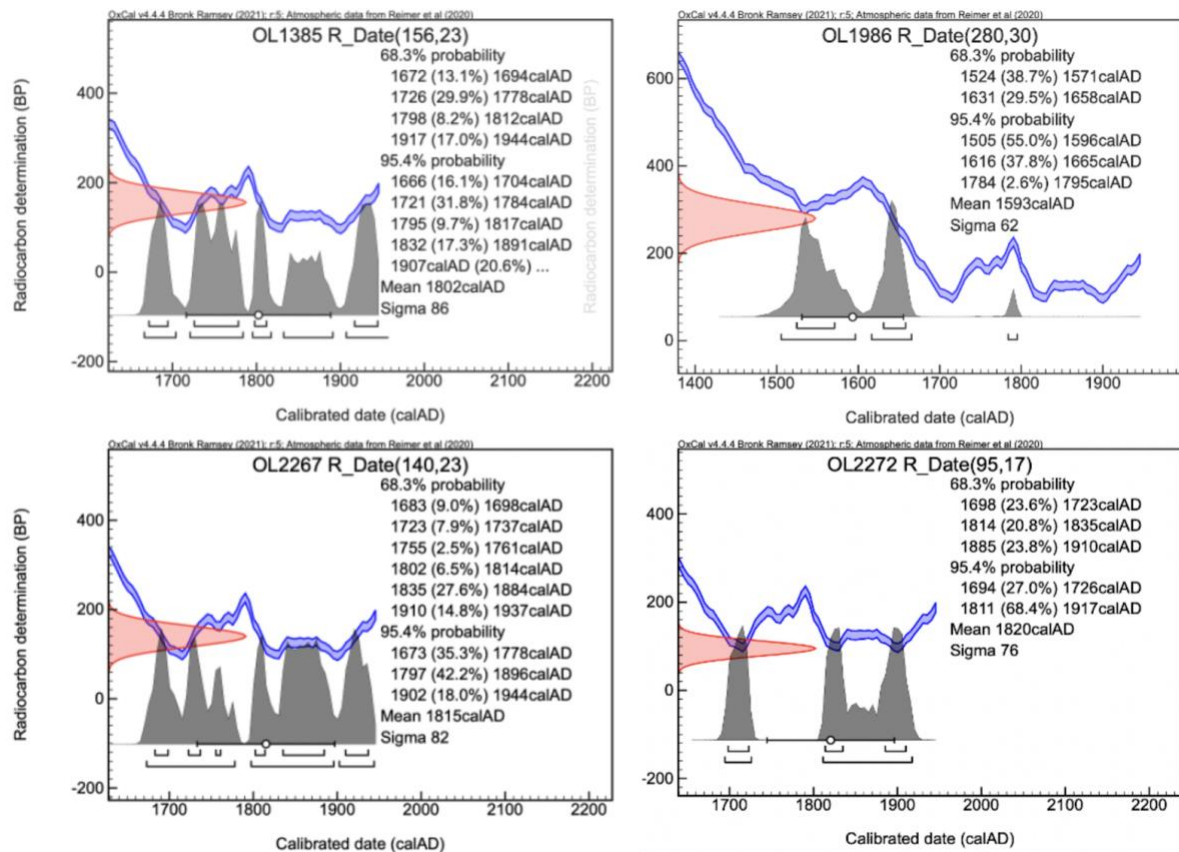
855 herpesvirus 1 (Herpesvirus of turkeys, accession: NC_002641.1) as an outgroup. Because of the large
856 distance between Meleagrid herpesvirus 1 and MDV strains, the tree is displayed as a cladogram with
857 branch lengths in black and bootstrap values in red. (B) As a comparison, the unconstrained
858 phylogeny was run in BEAST to allow the program to infer the root. BEAST determined the root to
859 be immediately prior to the earliest sample included in the run (OL1986, Spain, 1593CE).



861

862 **Fig. S7.**

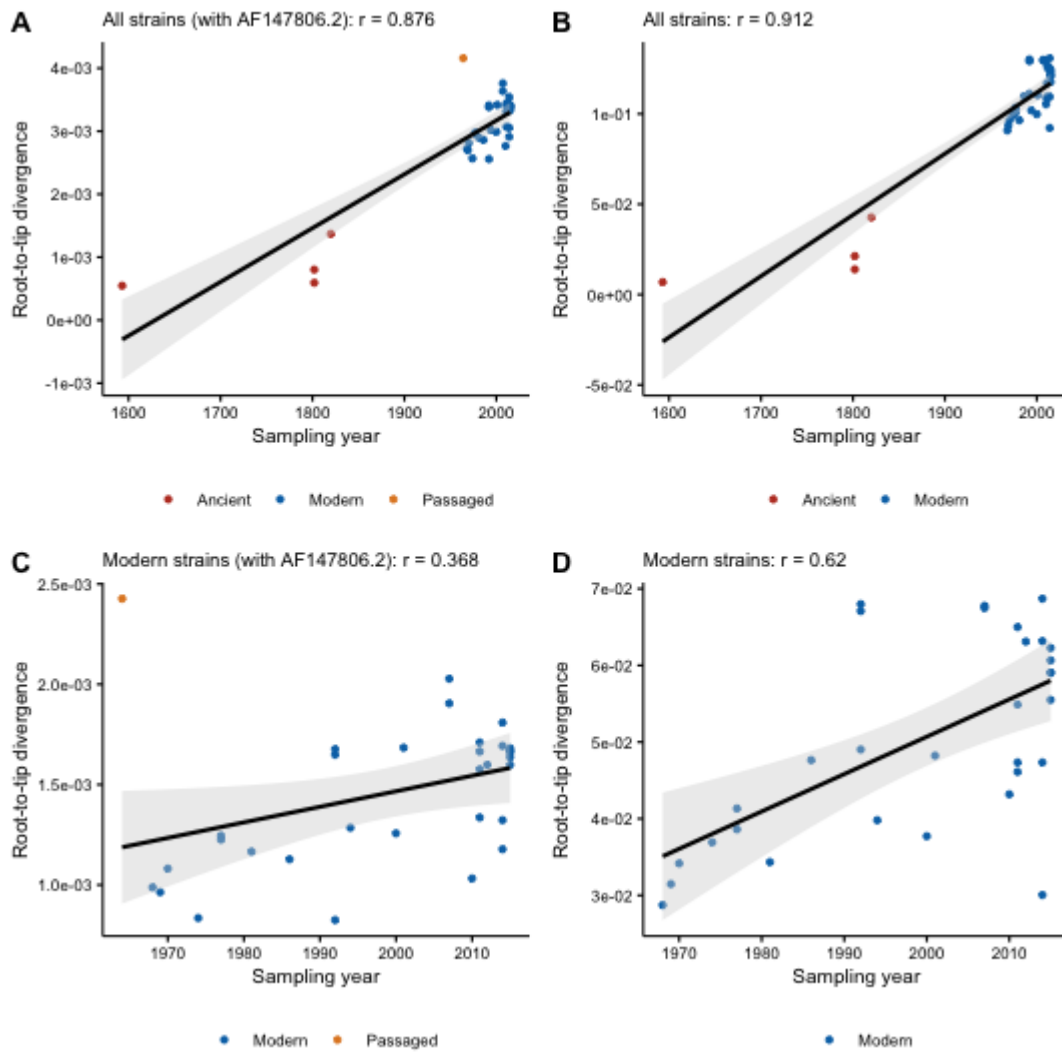
863 **Meq phylogeny showing ordered loss of tetraproline motifs.** The tree comprises 413 Meq
 864 sequences of the standard length (339aa) built using RAxML with 100 bootstrap replicates and
 865 visualized in iTOL(72). Around the edge, the integrity of each tetraproline motif is depicted (filled
 866 squares representing an intact tetraproline and open squares for a disrupted tetraproline). Meq
 867 sequences from ancient samples described herein are highlighted in gray, and the basal loss of the 6th
 868 tetraproline motif (common to all modern strains) is shown in bold. The label connected by a blue
 869 dotted line indicates the polymorphism that is found instead of tetraproline and the position of the
 870 tetraproline motif. For instance, '4 PAPP' indicates that the 4th tetraproline motif is disrupted by a
 871 proline-to-alanine substitution in the second proline position. '3 PP..P' denotes a deletion of the 3rd
 872 proline in the 3rd tetraproline motif.



873

874 **Fig. S8.**

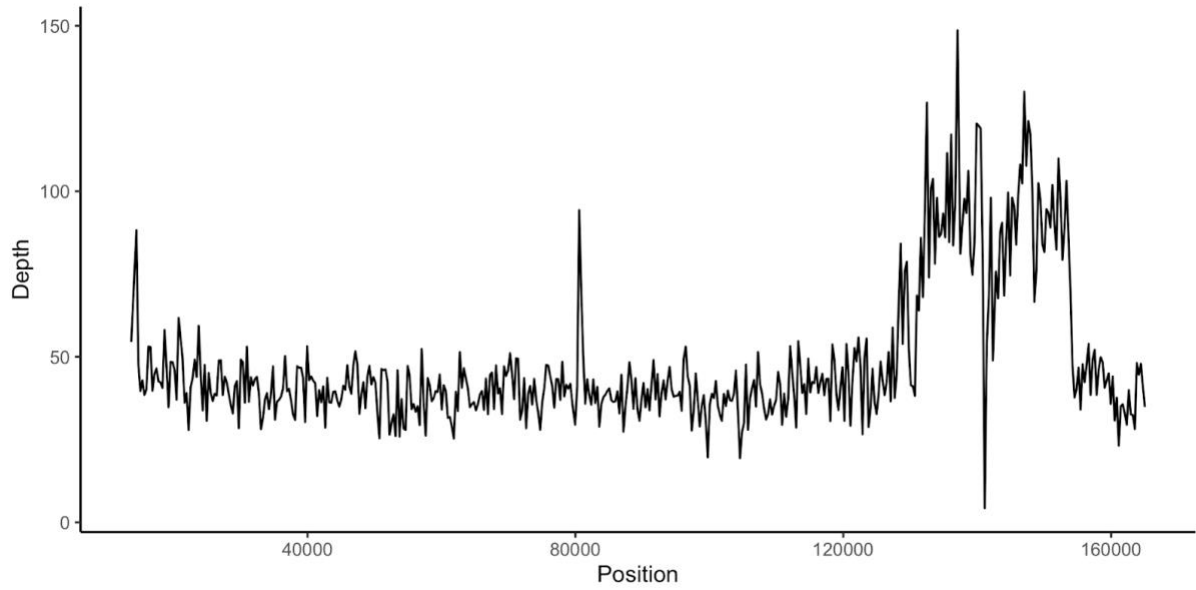
875 **Probability density plots for radiocarbon dating of ancient samples.** Calibration of dates was done
 876 in OxCal (<https://c14.arch.ox.ac.uk/oxcal.html>) using the IntCal20: Northern Hemisphere(37) method.



877

878 **Fig. S9.**

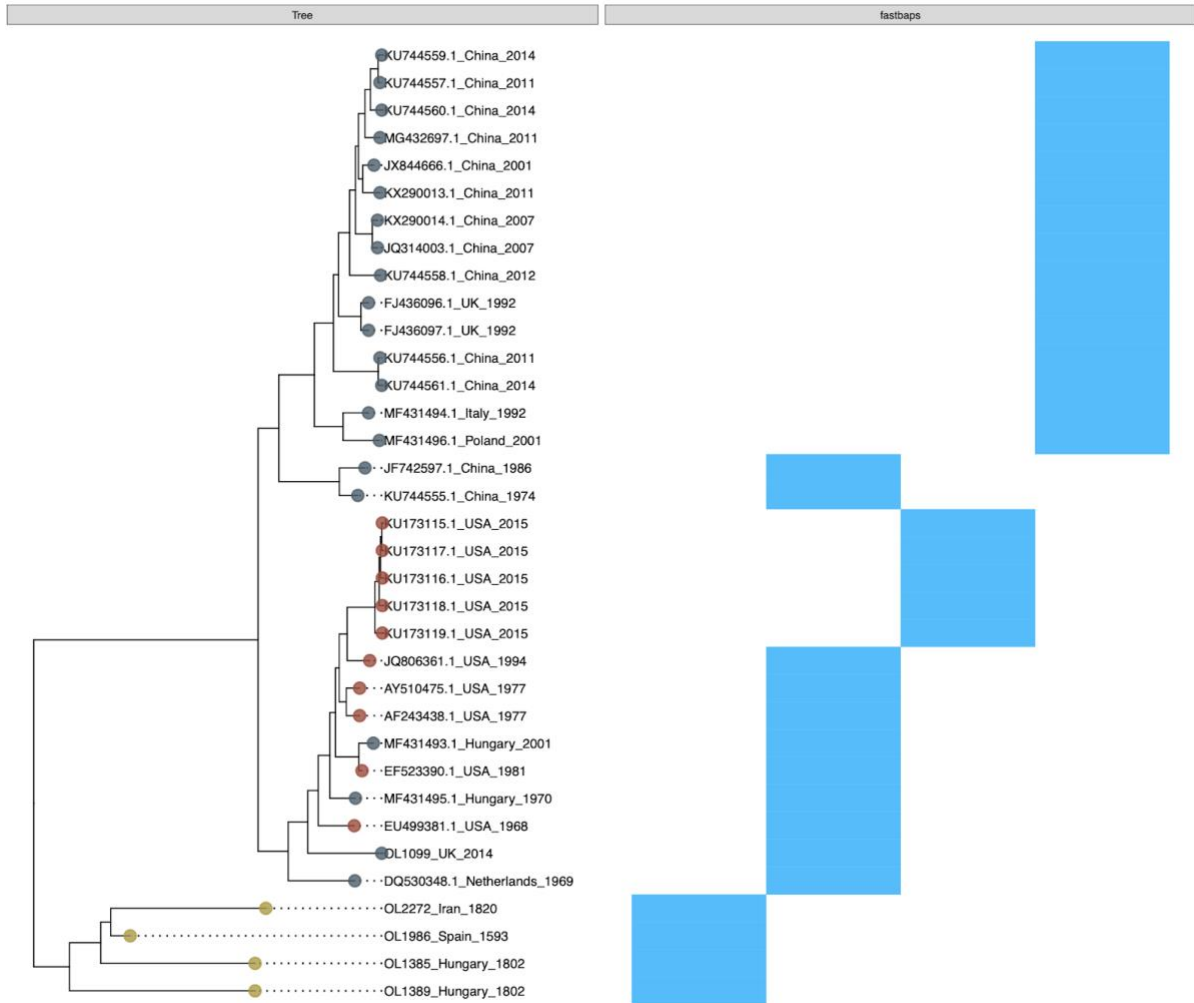
879 **Root-to-tip divergence against sampling date of Marek's Disease Virus strains and respective**
 880 **Pearson correlation coefficients.** (A) Ancient and modern strains (including AF147806.2, which was
 881 extensively passaged). (B) Ancient and modern strains (excluding AF147806.2). (C) Modern strains
 882 only (including AF147806.2) (D) Modern strains only (excluding AF147806.2).



883

884 **Fig. S10.**

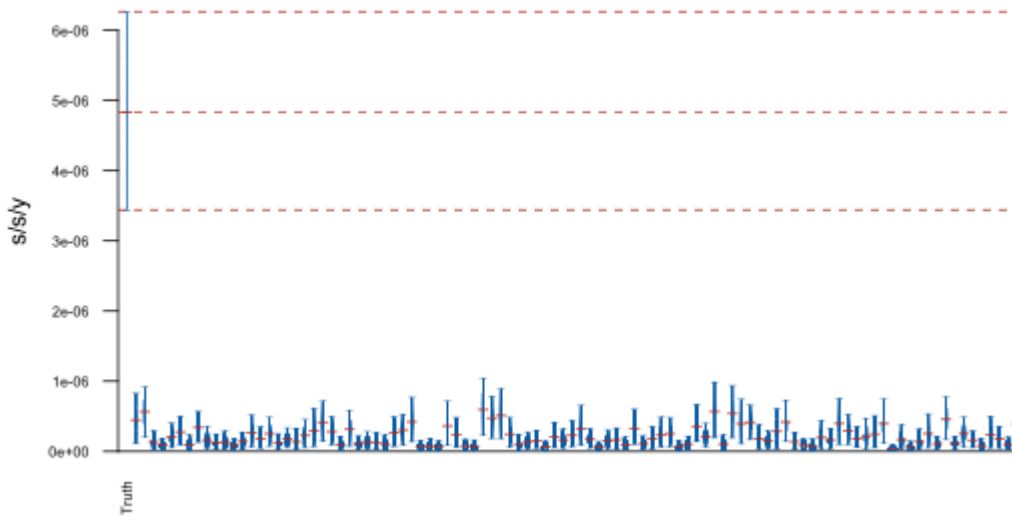
885 **Sequencing depth of the highest coverage ancient sample (OL1385).** Per-base sequencing depth
886 averaged over 300bp windows illustrating no significant drop-off in sequence depth across the
887 genome. The region of elevated coverage from ~130 kb is a duplicated region that encompasses the
888 internal repeat long (IRL) and the internal repeat short (IRS). The sharp decline in coverage at ~142
889 kb is a short repetitive region that was not baited.



890

891 **Fig. S11.**

892 **Phylogenetic clustering analysis using fastbaps.** Phylogenetic clusters (blue bars) were identified in
 893 the dataset using the fastbaps algorithm, under the baps prior model and unconstrained by a
 894 phylogenetic tree.



896

897 **Fig S12.**

898 **The Bayesian date randomization test (DRT) performed with 100 replicates, under a UCLD**
 899 **clock model in BEAST v1.10.4.** The plot shows the posterior distributions for the mean clock rate,
 900 using the true, unpermuted sampling dates (far left) and 100 replicates with sampling dates permuted
 901 among tips. Distributions are truncated at the upper and lower limits of the 95% HPD interval and
 902 horizontal red lines indicate the median estimates. The red dashed lines indicate the median and upper
 903 and lower limits of the 95% HPD interval of the clock rate inferred under the true sampling dates.

904 **Supplementary Tables**

905

906 **Table S4. Summary of estimated parameters from the ME and UCLD clock model BEAST**

907 **runs.**

908

Mean ages tip dating runs	UCLD (95% HPD Interval)
Root age	1602 (1486, 1768)
tMRCA(Modern)	1881 (1822, 1929)
tMRCA(American superclade)	1909 (1868, 1944)
tMRCA(Eurasian)	1904 (1854, 1945)
age OL1389	1737 (1669, 1858)
age OL1385	1752 (1672, 1871)
age OL1986	1675 (1627, 1801)
age OL2272	1799 (1701, 1910)
Mean clock rate (substitutions/site/year)	9.90E-6 (5.42E-6, 1.50E-5)

909

910 **Table S9.**

Strain	Year (CE)	Pathotype	Meq coding length	Sequence source
OL1385 (ancient)	1802 ± 86	Unknown	1020 bp	This study
RB1B	1981	Very virulent	1020 bp	EF523390.1
Md5	1977	Very virulent	1020 bp	NC_002229.3

911

912 **Meq sequences cloned for *in vitro* functional analysis.** Meq was cloned from the highest coverage

913 ancient sample (OL1385) as well as from two modern strains.

914 **Table S10.**

Sample	Country	Uncalibrated date (YBP)	Error +/-	Calibrated date	Error +/-	Laboratory	Lab Code
OL1385	Hungary	156	23	1802	86	Oxford RLAHA	OxA- 40466
OL2267	Iran	140	23	1815	82	Oxford RLAHA	OxA- 40467
OL2272	Iran	95	17	1820	76	Oxford RLAHA	OxA- 40491
OL1986	Spain	280	30	1593	62	Beta Analytic	Beta- 638008

915

916 **Radiocarbon dating of ancient chicken samples.** Raw dates were calibrated using IntCal20:917 Northern Hemisphere(37). See also [Figure S8](#) for probability density plots.918 **Data S1.**

- 919 ● **Table S1: Sample metadata.** Metadata for all ancient samples sequenced in the present
- 920 study.
- 921 ● **Table S2: Screening and capture sequencing results.** Sequencing statistics for all MDV-
- 922 positive screened samples that were then submitted for in-solution capture.
- 923 ● **Table S3: Modern genome metadata.** Metadata for all modern MDV sequences included in
- 924 phylogenetic analyses.
- 925 ● **Table S6: Fixed differences between ancient and modern MDV strains.** Table of single
- 926 nucleotide polymorphisms found to be fixed between ancient strains (with at least 2
- 927 representatives) and modern strains.
- 928 ● **Table S7: PAML results.** Results from the branch-site analysis of positive selection.
- 929 ● **Table S8: Meq metadata.** Metadata of all Meq sequences included in the Meq analysis, plus
- 930 additional information about the tetraproline content for each sequence.
- 931 ● **Table S11: Pre-capture metagenomic IDs.** Summary of the pre-capture HAYSTAC results.
- 932 ● **Table S12: SNP summary table.** Summary table of all SNPs and depth of coverage in all
- 933 ancient samples.
- 934 ● **Table S13: BEAST tip dates.** Tip dates used as priors in the BEAST analysis.